Atomic Structure and Dynamics of Single Pt Atom Interactions with Monolayer MoS_2

Huashan Li[1†], Shanshan Wang[2†], Hidetake Sawad[2,3,4], Grace Ggoch Ddeul Han[1], Thomas Samuels[2] , Christopher S. Allen[2,4], Angus I. Kirkland[2,4], Jeffrey C. Grossman[1], Jamie H. Warner[2*]*

[1]Department of Materials Science and Engineering, Massachusetts Institute of Technology, 77 Massachusetts Avenue, Cambridge, MA, 02139, USA.

[2]Department of Materials, University of Oxford, Parks Road, Oxford, OX1 3PH, United Kingdom

[3]JEOL Ltd., 3-1-2 Musashino, Akishima, Tokyo 196-8558, Japan

[4]Electron Physical Sciences Imaging Center, Diamond Light Source Ltd, Didcot, Oxfordshire, OX11 0DE, United Kingdom

*Jamie.warner@materials.ox.ac.uk; jcg@mit.edu; †Equal contribution

Abstract

We have studied atomic level interactions between single Pt atoms and the surface of monolayer MoS_2 using aberration-corrected annular dark field scanning transmission electron microscopy at an accelerating voltage of 60kV. Strong contrast from single Pt atoms on the atomically resolved monolayer MoS_2 lattice enables their exact position to be determined with respect to the MoS_2 lattice, revealing stable binding sites. In regions of MoS_2 free from surface contamination, the Pt atoms are localized in S vacancy sites and exhibit dynamic hopping to nearby vacancy sites driven

by the energy supplied by the electron beam. However, in areas of MoS_2 contaminated with carbon surface layers, the Pt atoms appear at various positions with respect to the underlying MoS_2 lattice, including on top of Mo, and in off-axis positions. These variations are due to the Pt bonding with the surrounding amorphous carbon layer, which disrupts the intrinsic Pt-MoS_2 interactions, leading to more varied positions. Density functional theory (DFT) calculations reveal that Pt atoms on the surface of MoS_2 have a small barrier for migration and are stabilized when bound to either a single or double sulfur vacancies. DFT calculations have been used to understand how the catalytic activity of the MoS_2 basal plane for hydrogen evolution reaction (HER) is influenced by Pt dopants by variation of the hydrogen adsorption free energy. This strong dependence of catalytic effect on interfacial configurations is shown to be common for a series of dopants, which may provide a means to create and optimize reaction centers.

KEYWORDS: Pt dopants, MoS2, ADF-STEM, 2D materials

The presence of single isolated atom impurities and dopants either on the surface or directly bonded within the lattice structure of 2D materials influences the properties.[1-10] Understanding the atomic structure that defines the bonding between single foreign atoms and the host 2D crystal is critical for developing accurate models that can predict the impacts of doping. Single metal atom doping of materials has also found significant recent interest in the development of new catalysts by reducing the mass content of precious metals such as Pt, whilst maintaining high performance.[11-13] A key aspect to single metal atom catalysts is preventing aggregation of the active species into clusters, reducing the loss of metal atoms by detachment, and providing the optimum bonding configuration for catalytic activity. Recent work has shown that doping 2D layered MoS_2 can lead to higher activities in the hydrogen evolution reaction, utilizing Co, Ni and

Pt single metal dopants.[14,15] MoS_2 is normally only active at edge sites, but the incorporation of isolated metal substitutional or surface dopants can activate the basal plane and lead to a large increase in the number of active catalytic sites. Therefore, resolving the atomic structure of single metal atoms and their structural interaction with MoS_2 helps reveal the stable configurations that dictate the catalytic performance.

Aberration-corrected electron microscopy (AC-TEM), in both phase contrast TEM (AC-TEM) and annular dark field scanning transmission electron microscopy (ADF-STEM) modes have been shown to be key methods for directly imaging single metal dopants in nanoscale materials. When combined with electron energy loss spectroscopy (EELS) it is possible to map elemental composition at the single atom level.[16-18] The z-dependent contrast in ADF-STEM results in bright contrast at heavy single metal atom sites, such as Au, on the surface or within the lattice of lighter elemental materials such as graphene or MoS_2.[19] Au atoms on the surface of MoS_2 have been observed on a range of atomic sites, such as on top of S, Mo and hollow sites.[19] Recent work using ADF-STEM and EELS has further revealed that Cr and V dopants are often present in chemical vapor deposition (CVD) grown MoS_2, where the Cr/V dopants directly substitute Mo atoms.[20]

The surface of 2D materials such as graphene and MoS_2 typically contain patches of amorphous carbon and this modifies the local surface chemistry. Deposition of metal atoms onto graphene results in preferential adhesion to the amorphous region, which makes it difficult to study intrinsic 2D-metal interactions. Recent work using *in-situ* high temperature heating in AC-TEM to remove the amorphous carbon residue to study the epitaxial interactions between gold nanoclusters and graphene has shown different behavior compared to amorphous carbon surfaces.[21] Extending this approach to the single atom level in a variety of 2D materials will reveal

insights into single metal atom behavior for a diverse range of applications, including photonics and catalysis with MoS_2. For MoS_2 monolayers, amorphous surface carbon will be hard to image against the MoS_2 layer. However, using ADF-STEM at a lower accelerating voltage of 60kV should enable contrast differentiation between clean and contaminated regions and hence enable imaging of single metal atom dopant structure in each of these regions. Many of the studies have involved metal dopants incorporated at the synthesis stage, rather than post-synthesis deposition. Clear unambiguous atomically resolved structure of single Pt atoms on the surface of clean MoS_2 has yet to be achieved, where both 2S and Mo columns are discriminated, S vacancies are identified, and the detailed Pt bonding to the MoS_2 is evident in the images. Such information will help further understanding of this hybrid system for future catalytic applications.

Here, we have used monolayer MoS_2 grown by CVD as an ideal clean transition metal dichalcogenide (TMD) substrate to deposit a Pt precursor from solution to form a hybrid Pt-MoS_2 system and to study the detailed atomic structure of the species formed using ADF-STEM at an accelerating voltage of 60kV to minimize S vacancy production. S vacancies are still produced, but at a lower rate than at higher voltages. We have located single Pt atoms in both clean and carbon contaminated regions of MoS_2 and have directly resolve the atomic structure of the Pt binding sites relative to the MoS_2 lattice. Dynamics of Pt diffusion across the clean MoS_2 surface have been captured at room temperature, where energy is supplied by the electron beam. Comparisons of the site location of Pt atoms in these two regions shows that Pt on clean MoS_2 is positioned at S sites, whereas Pt in contaminated carbon regions are located at random sites relative to the MoS_2 lattice. This is due to Pt-C bonding that influences the structure, compared to the clean MoS_2 region where intrinsic Pt surface migration dominates. Density functional theory (DFT) calculations of the relative binding energies of Pt to different sites on the surface of MoS_2 show

that S vacancies are required to trap Pt in a location. While trapped Pt atoms tend to suppress the activity of S vacancy, Pt dopants on a defect-free MoS_2 sheet may serve as catalytic centers for HER.

Results and Discussion

Monolayer MoS_2 grown by CVD was transferred to a SiN TEM grid using a PMMA support layer and cleaned by thermal annealing. Small thin residual carbon patches found on the MoS_2 are most likely from the PMMA. After initial AC-TEM inspection to ensure the sample was free from a substantial carbon contamination and had significant regions of pristine MoS_2 visible, a drop of Pt precursor solution was deposited onto the grid and allowed to dry in air. The sample was then heated under Ar gas flow at 350^{o}C to decompose the Pt precursor and produce Pt on the surface of MoS_2. Some of the Pt had aggregated into small nanoclusters, figure 1(a)-(c), and energy dispersive X-ray spectroscopy confirmed they contain Pt, figure S6. There are also individual Pt atoms distributed across the sample and some few-atom clusters, figure S2. Some of the isolated Pt atoms adhered to the surface amorphous carbon, which is visible with higher contrast in figure 1(b) and 1(c). Figure S1 also shows Pt atoms bound to carbon contamination regions. However, Pt atoms are also found in the pristine regions of MoS_2, away from the amorphous carbon regions, as shown in figure 1(d).

The ADF-STEM image shown in figure 1(e), is a magnified view from the yellow boxed region in figure 1(d), showing a single Pt atom on MoS_2. Contrast in an ADF-STEM image is larger for higher atomic number elements/columns, enabling the discrimination of the Mo and 2S columns in the MoS_2 image in figure 1(e), which shows a Pt atom located in a S column site. We have imaged more than 10 individual Pt atoms residing in the clean areas of MoS_2 and all showed the same structure of Pt atoms located in S sites. Figures S4 and S5 show two more examples. The

atomic model in figure 1(f) shows a schematic 3D view of a Pt atom replacing two S atoms, i.e located at a 2S vacancy (S-sub configuration).

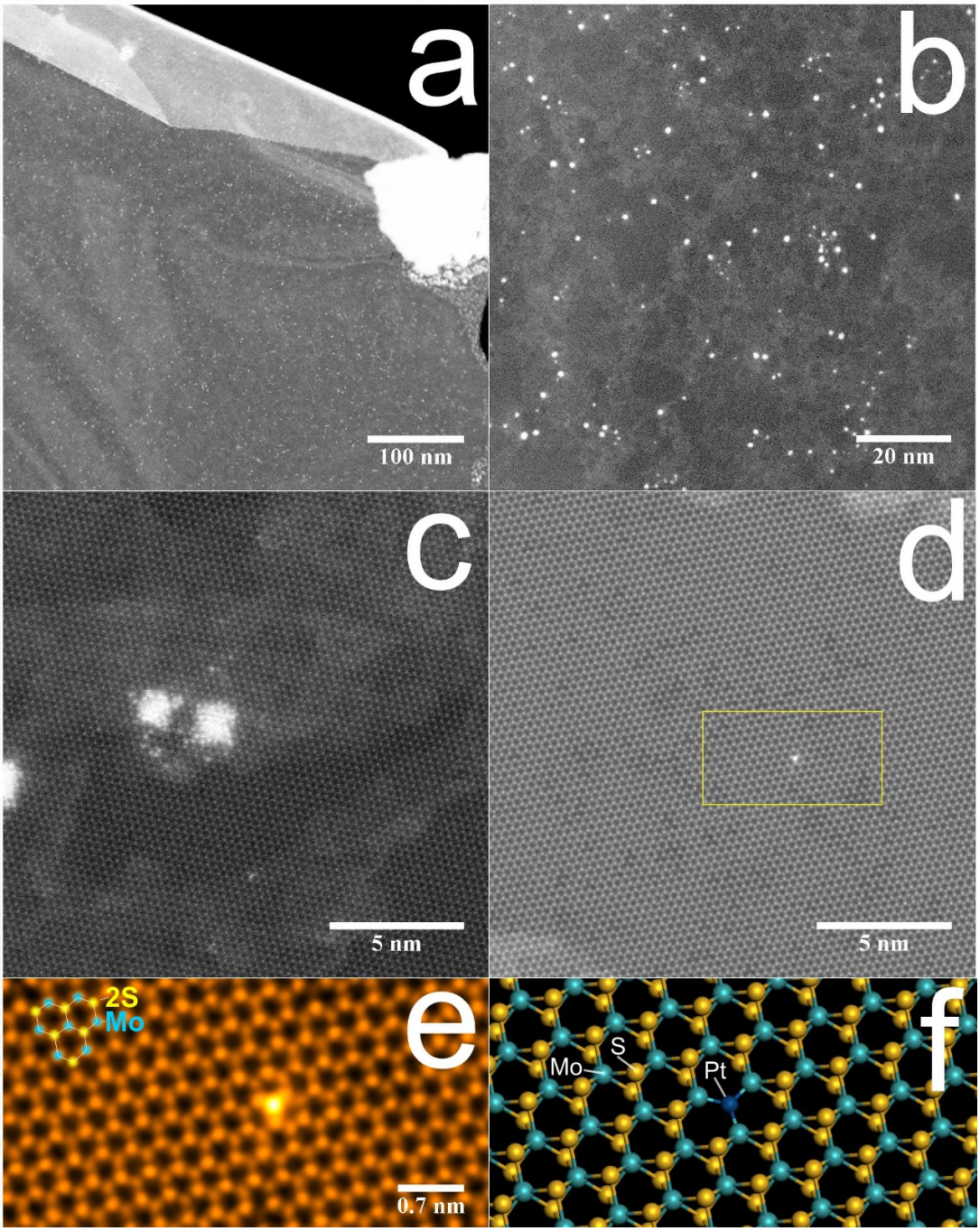

Figure 1 ADF-STEM images of Pt on monolayer MoS_2. (a) Low magnification image showing Pt nanoparticles on the surface of MoS_2. (b) and (c) Higher magnification images showing Pt nanoclusters and

single Pt atom species on the surface of MoS_2. (d) Atomic resolution image showing a single Pt atom located in the clean region of MoS_2 (e) Enlarged image from the boxed region in (d), (orange false colour), showing strong contrast from a single Pt atom located in a S lattice site. (f) DFT relaxed atomic model showing a Pt atom in a 2S vacancy site.

ADF-STEM imaging at an accelerating voltage 60kV of the single Pt atom (figure 1(d) and (e)) caused migration across the surface of MoS_2 before being trapped at other sites for fixed durations, with energy supplied from the electron beam. Figure 2 shows a sequence of ADF-STEM images in which the hopping of a single Pt atom to 5 different sites is observed, all of which are S lattice sites, further confirming the preference for Pt to bind to S positions rather than Mo sites on a clean surface. The apparent double image of a Pt atom in figure 2(b) is due to the electron beam causing the Pt to hop during the raster scanning image formation process. Small white circles are used to indicate the Pt atom's prior position. This type of dynamics is typical for atomic scale systems imaged by TEM, where we only capture the positions of fixed stability between the rapid motion. Figure 2(g) shows a smoothed magnified image of the Pt atom from figure 2(a), showing the Pt sits at the S site, but also the presence of S vacancy to the top right, evident by the reduced contrast. Figure 2(h) shows the migration of the Pt atom schematically illustrated on a MoS_2 lattice, revealing a random direction, even though the electron beam is scanning. Further insights into this dynamic behavior are gained by using density functional theory to calculate the energy barriers for migration of Pt atoms on the surface of MoS_2.

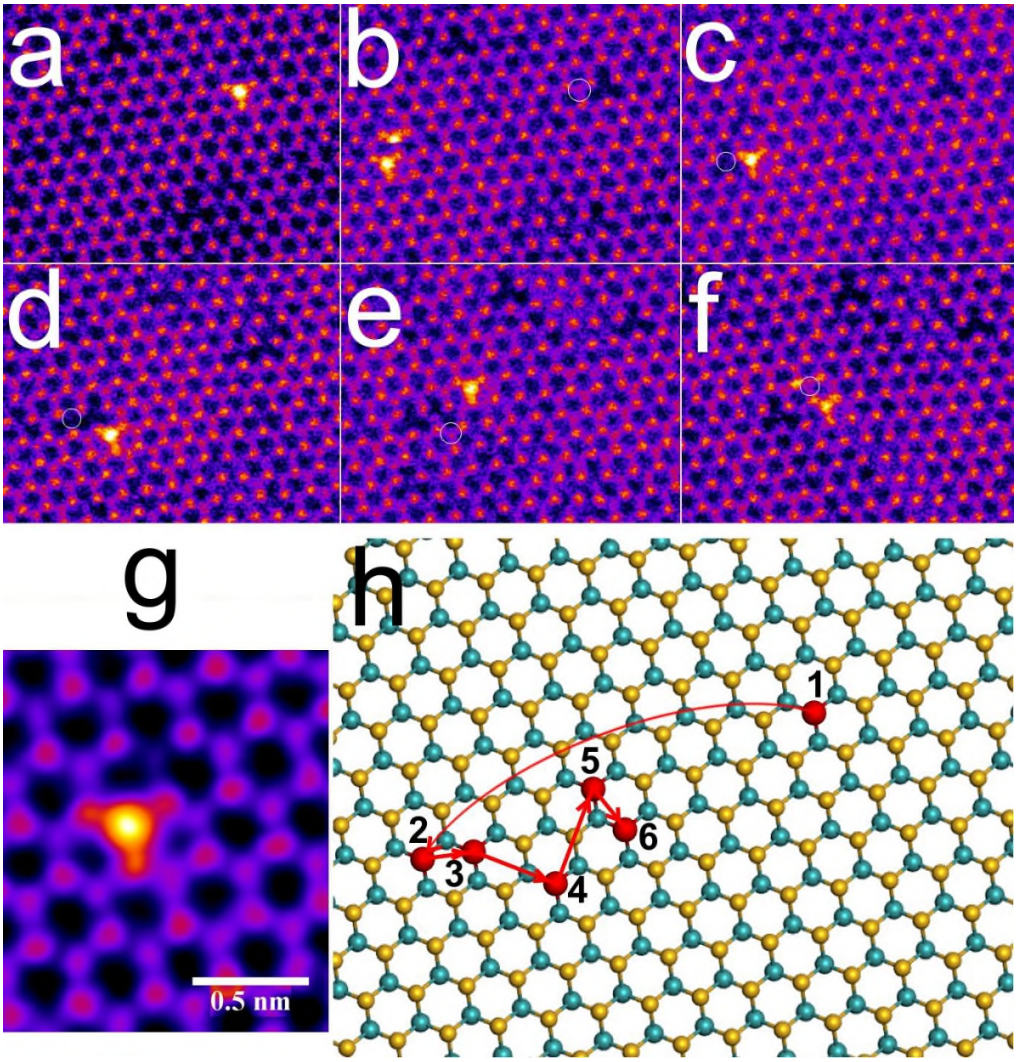

Figure 2. Dynamics of Pt atom migration across the surface of MoS_2. (a)-(f) Sequence of ADF-STEM images (false colour LUT 'fire') capturing the movement of a single Pt atom on MoS_2. White circles indicate the prior location. (g) Magnified ADF-STEM image of the Pt atom in (a), showing the Pt sitting in the S site location and the presence of a S vacancy. (h) Schematic illustration of Pt migration on a MoS_2 surface.

Image simulations, figure 3(e)-(g), were performed based on DFT relaxed atomic models, figure 3(a)-(c), and were compared to an experimental ADF-STEM image of Pt on MoS_2, figure 3(d). Line profiles, figure 3(i), shows a good contrast match between the experimental image in figure

3(d) and the simulation of a Pt atom in the 2S vacancy, figure 3(c) and (g). The contrast in the image simulations and experimental images were normalized to that in the Mo column. The contrast from the Pt region is substantially less than that predicted from simulations for Pt on top of 2S atoms, and therefore we conclude that the Pt is residing within a vacancy defect in the ADF-STEM images.

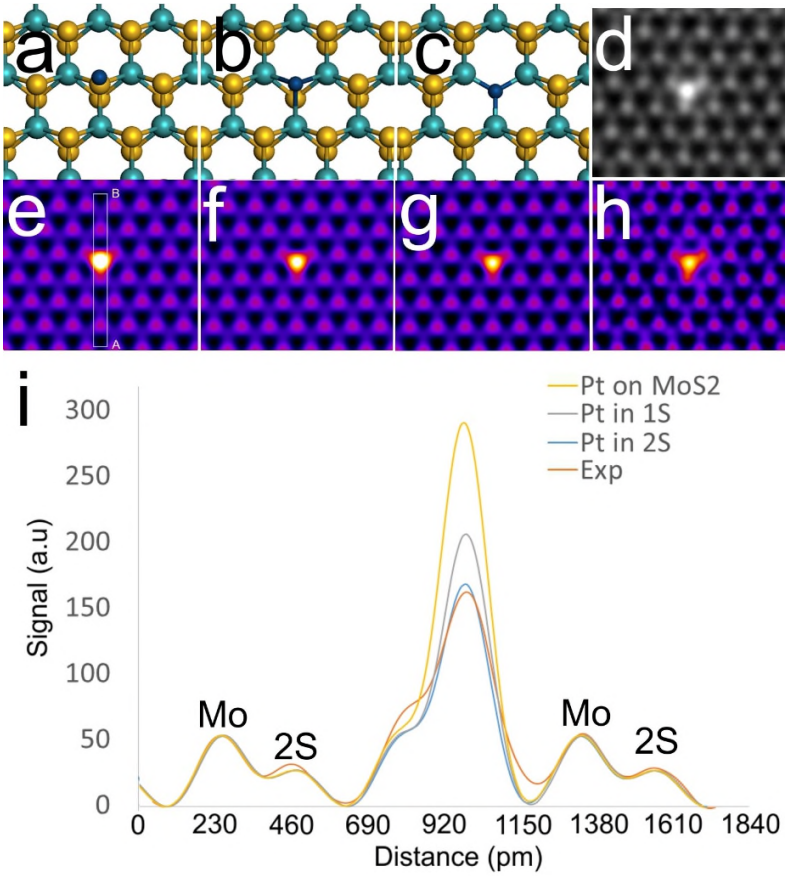

Figure 3. Image simulations of Pt atom in different configurations. (a)-(c) Atomic models for (a) Pt on top of 2S, (b) Pt in a 1S vacancy, and (c) Pt in a 2S vacancy. Tilt is introduced to show the 2S atoms. (d) Experimental ADF-STEM image of a Pt atom on MoS_2 in greyscale. (e)-(g) ADF-STEM image simulations based on the models shown in (a)-(c) respectively. Colour LUT 'fire' is used to highlight the contrast associated with the Pt atom. (h) Processed image from (d) with colour LUT 'fire' used for comparison to image simulations. (i) Boxed line profiles taken from the greyscale images of (e)-(h) respectively across

the region indicated by the white box in (e) from A-B direction. Plots are normalized to the Mo column intensity for relative comparison.

The energy barrier for a Pt atom to migrate across the surface of pristine MoS_2 is calculated in figure 4, for two different pathways, by the valley site (V-top figure 3(a)-(d)), or by the S atom (S-top figure 3(e)-(h)). Both pathways have small DFT energy barriers of ~0.6-0.82 eV, which indicates that Pt atoms can diffuse easily across the surface of defect free MoS_2 at room temperature. Binding energies were calculated by DFT for Pt at sites: S-top = 3.22eV, Mo-top = 3.71eV and V-top = 3.17eV. However, the energy barrier for migration is significantly different if the Pt atom is located within a S vacancy.

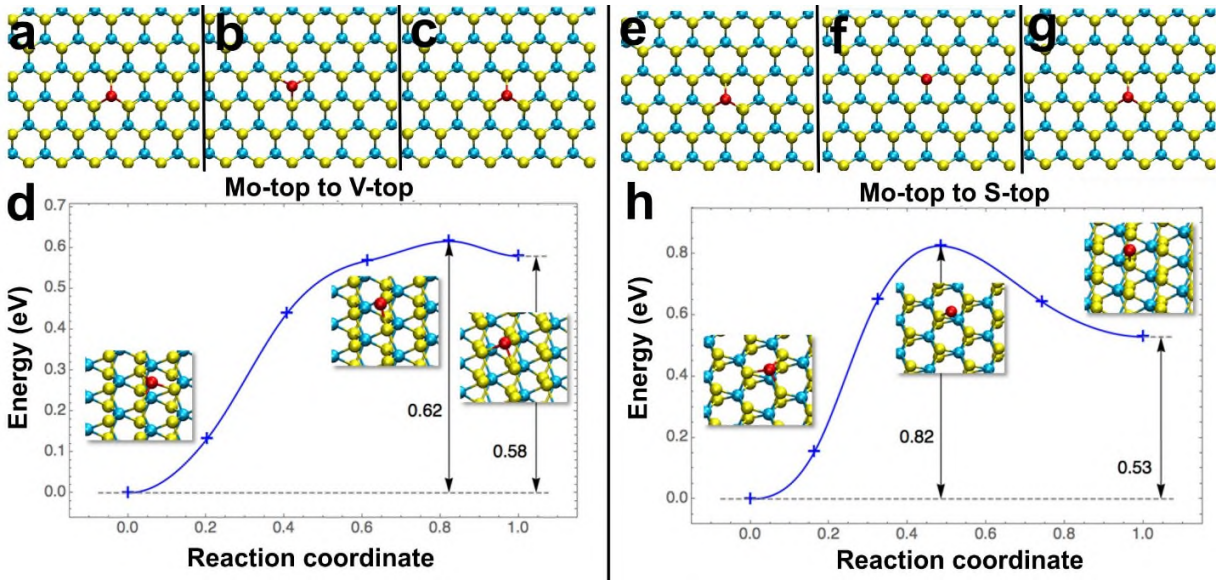

Figure 4 DFT calculations for a single Pt atom migrating across a pristine MoS_2 surface for two different pathways. (a)-(c) Mo-top site to valley site (V-top) to Mo-top site. (d) Energy as a function of reaction coordinate for pathway (a)-(c). (e)-(g) Mo-top site to S-top site to Mo-top site. (h) Energy as a function of reaction coordinate for pathways (e)-(g).

Figure 5 shows the energy barriers needed for a Pt atom to escape from a single S vacancy to the MoS_2 surface by three different pathways, Mo atom (figure 5(b)), V-top (figure 5(c)), and S-top (figure 5(d)). All pathways show similar escape energy barriers of ~3eV and small barriers (<0.5 eV) for backward hopping, leading to an extremely large unbalance between forward and backward transitions (rate ratio $>10^{45}$ based on the Arrhenius' equation), which indicates that the presence of the S vacancy in MoS_2 acts as a stable trapping site to localize Pt atoms. This also supports the experimental observations in figure 1 and 2, where Pt is predominantly observed in the S site. The same behavior is expected for Pt in a 2S vacancy, which exhibits a similar structure with a slightly smaller binding energy (5.74 eV) compared to that for Pt in a S vacancy (6.08 eV).

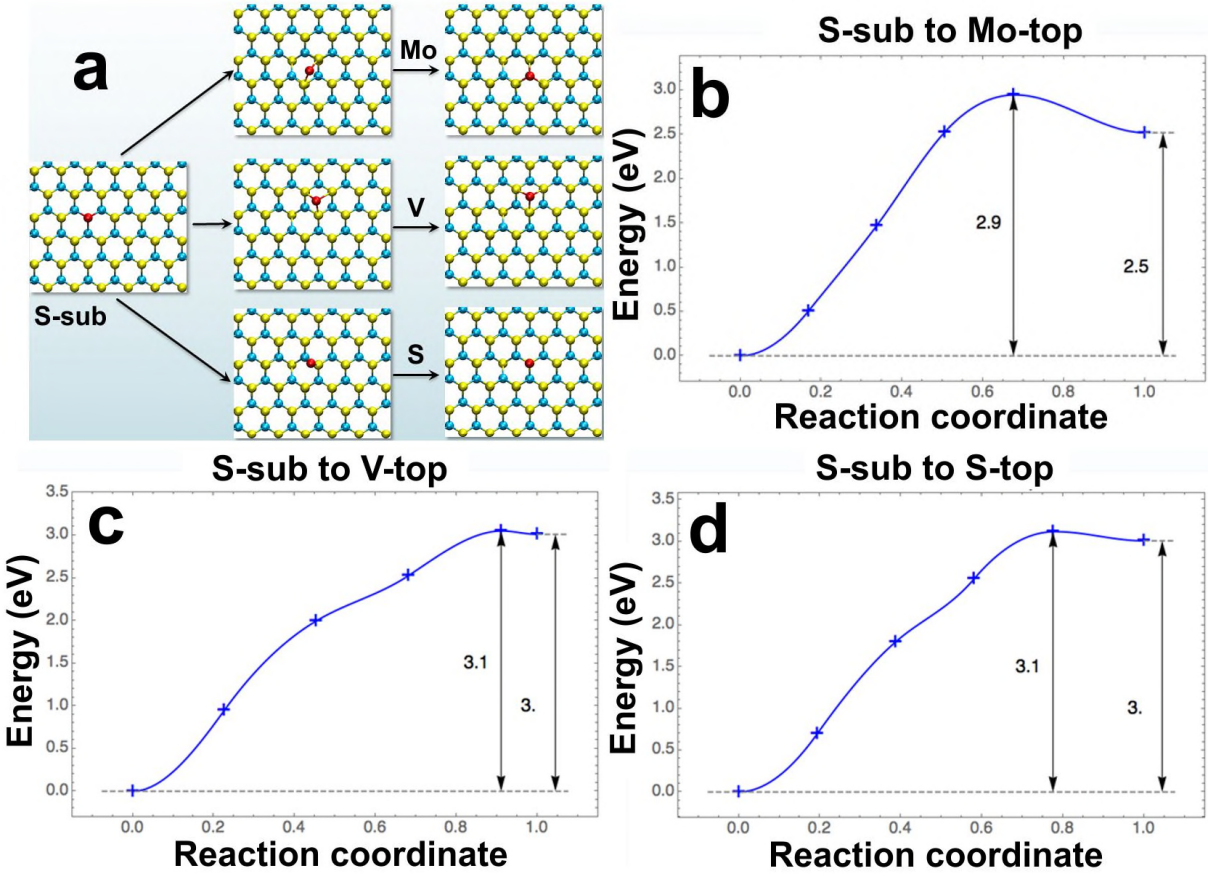

Figure 5. DFT calculations for a single Pt atom escaping from a S vacancy across MoS_2 surface for three different pathways. (a) By Mo-top site, V-top site and S-top site. (b) Energy as a function of reaction coordinate for the Mo-top site pathway. (c) Energy as a function of reaction coordinate for the V-top site pathway. (d) Energy as a function of reaction coordinate for the S-top site pathway.

These dynamics of Pt atom hopping between stable sites indicates that the Pt atoms find new S vacancy sites in the MoS_2. The electron beam is known to induce S vacancies in MoS_2, even at 60kV accelerating voltage and these are mobile in the lattice, leading to assembly into line vacancy structures.[22-25] Therefore, during the imaging in figure 2, S vacancy sites are constantly being created and migrating. Consistent with existing literature,[26] our calculated formation energy of a S vacancy is 6.87 eV, which is much higher than the binding energies of a Pt atom on top of pristine MoS_2 and similar to those trapped at a S vacancy. Hence, the high flexibility of S atoms is likely to arise from the efficient energy transfer between electron beam and light atoms.[27] Based on the inelastic model including exact relativistic kinematics,[27] the maximum energies transferred from a 60 kV electron to S, Mo, Pt atoms are 4.35, 1.45, 0.71 eV, which provides sufficient energies for S/Pt diffusion and explains the relatively slow S ejection observed in experiments.

In figure 6, DFT calculations demonstrate the role of S vacancy migration on the Pt stability. Figures 6(a)-(c) show a 2.3eV energy barrier for S vacancy migration, and in figures 6(d)-(f) the barrier remains similar, even though a Pt atom is located next to the S vacancy site. This indicates that there is no preference for S vacancies to migrate next to Pt atoms in MoS_2. However, the presence of a S vacancy next to a Pt atom in a 1S vacancy site lowers its energy barrier for hopping to the next site to 0.75eV, which is considerably less than the ~3eV required for Pt to migrate to the surface sites in figure 5. This indicates that S vacancy migration to sites next to Pt atoms in 1S vacancy sites will enhance the migration dynamics of the Pt atoms across the MoS_2.

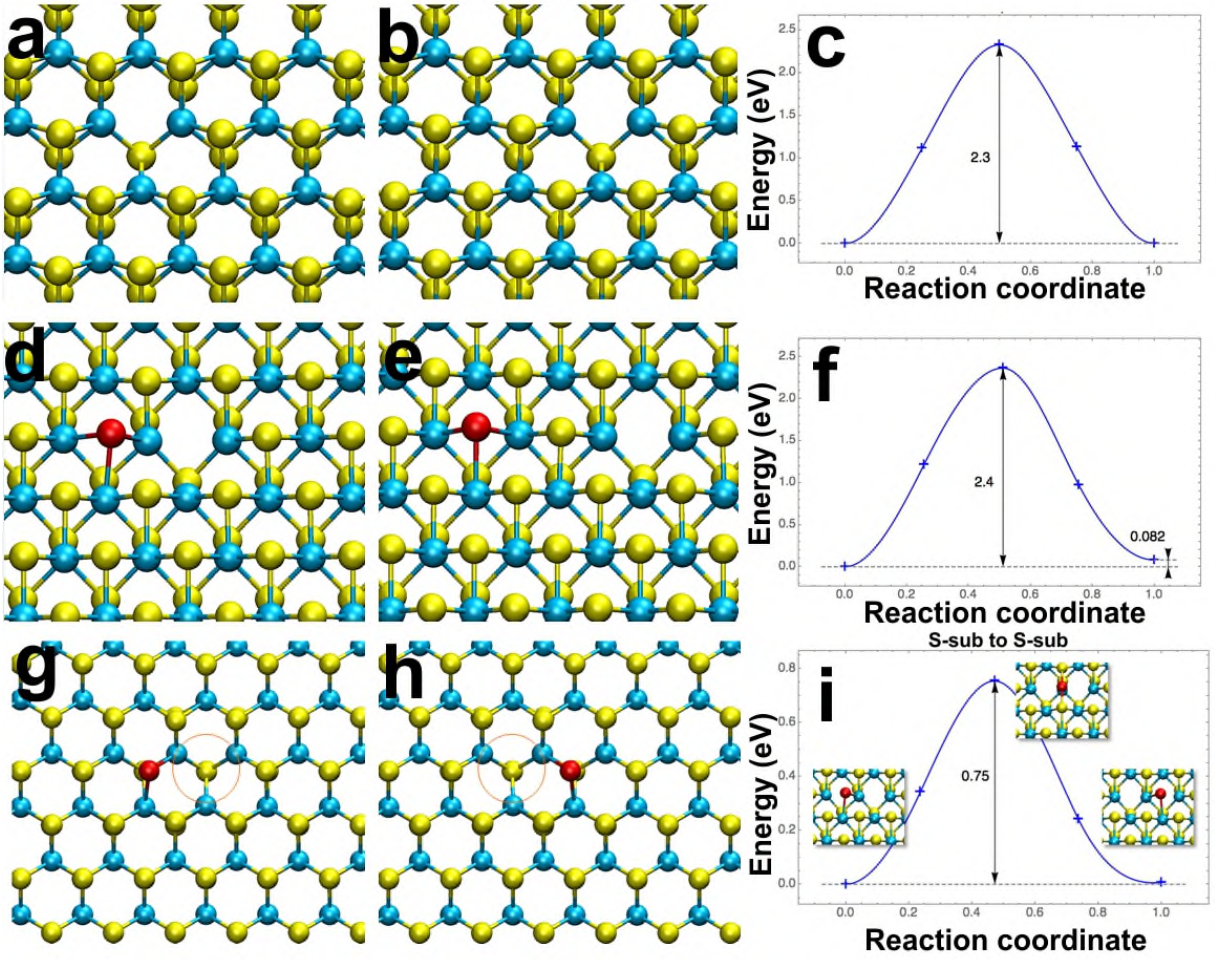

Figure 6 DFT calculations for S vacancy migration and Pt migration with S vacancy assistance. (a)-(b) Atomic models showing a S vacancy moving one site to the right. A slight tilt is introduced in the model to show the two S atoms. (c) Energy as a function of reaction coordinate for the S vacancy migration pathway shown in (a)-(b). (d)-(e) Atomic models showing S vacancy moving one site to the left, next to a Pt atom sitting in a S vacancy site. A slight tilt is introduced in the model to show the two S atoms. (f) Energy as a function of reaction coordinate for the S vacancy migration pathway towards Pt atom shown in (d)-(e). (g)-(h) Atomic models showing a Pt atom migrating to the S vacancy site to its right. The S vacancy is indicated by orange circle. (c) Energy as a function of reaction coordinate for the Pt atom migration from one vacancy to the next by the pathway shown in (g)-(h).

The presence of surface amorphous carbon on top of MoS_2 also plays an important role in the relative structure of Pt:MoS_2. Strong Pt-C bonding impacts the intrinsic Pt:MoS_2 interactions and leads to a wide range of positions adopted by the P atom relative to the MoS_2 lattice. Figure 7(a) shows a single Pt atom located in a region of MoS_2 with significant surface carbon. The yellow box shows the boundary between the clean MoS_2 on the right and the contaminated region to the left. A line scan of the intensity from the ADF-STEM image, figure 7(c), shows a steady increase in the background level after 1nm going from pristine to the area containing the carbon. This increase in background signal from the carbon indicates thicker regions. Figures 7(d)-(i) show a series of ADF-STEM images of the dynamics of the Pt atom in figure 7(a), with the Pt changing its relative position with respect to the MoS_2 lattice across the three frames. The coordination of the Pt atom is random and is mainly dictated by the bonding in the carbon.

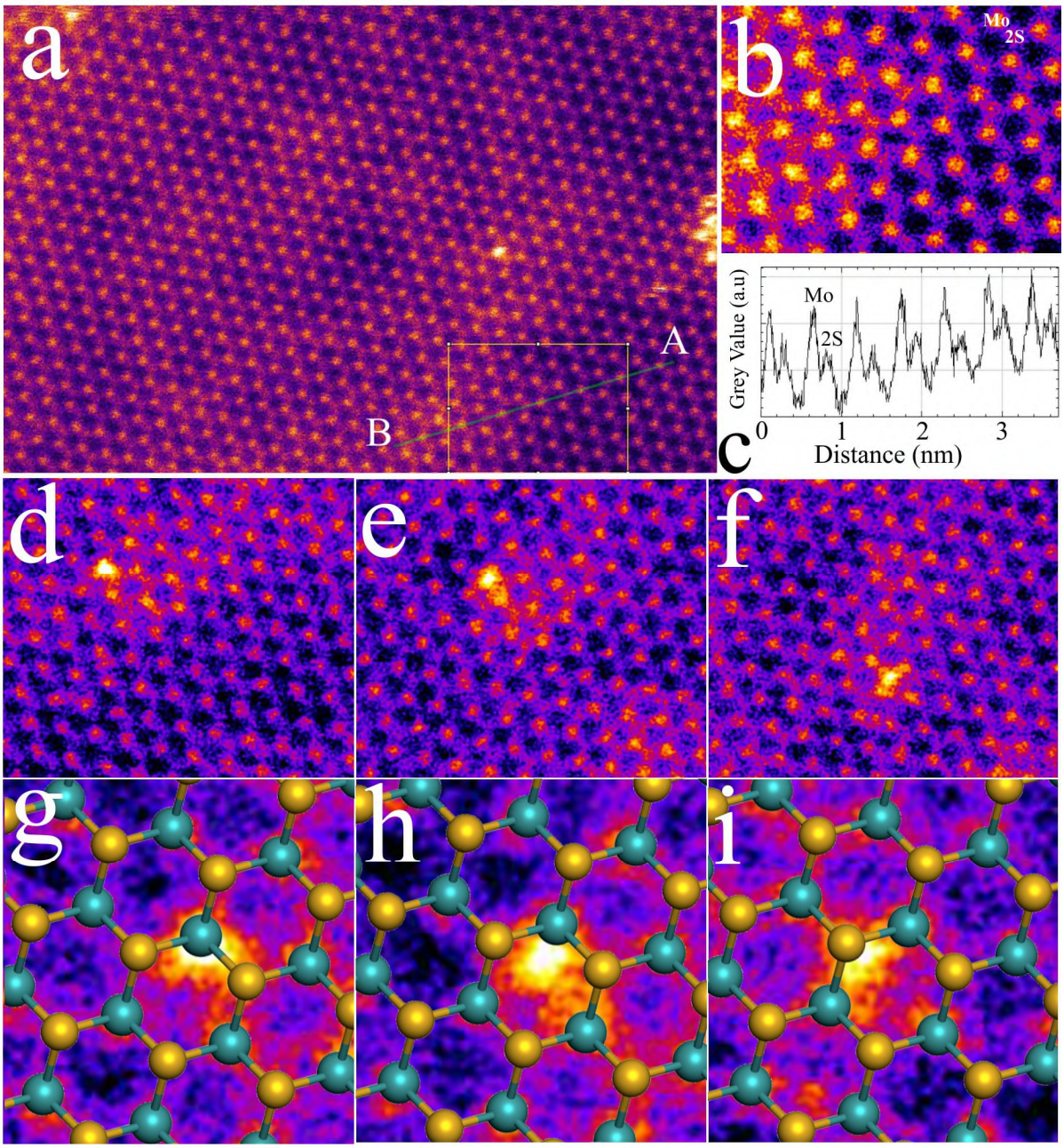

Figure 7. Pt atoms in regions of MoS_2 with surface carbon contamination. (a) ADF-STEM image (false colour LUT 'fire') showing a single Pt atom in a contaminated region of MoS_2. (b) Magnified view of the region indicated in (a) with the yellow box, showing the interface between the clean and contaminated area. (c) Line profile of intensity as a function of distance along the line indicated in green in (a), from A-B. Mo and 2S columns are indicated and a rising background is seen in the presence of the amorphous carbon

surface layer. (d)-(f) Series of ADF-STEM images showing the dynamics of a single Pt atom. (g)-(i) Overlay of MoS_2 atomic positions with the ADF-STEM images in (d)-(f) respectively, showing the Pt atom is randomly located with respect to the Mo and S sites.

Figure 8(a) shows an atomic model of monolayer MoS_2 with a small surface region of amorphous carbon containing three Pt atoms (blue). The ADF-STEM image simulation of the structure in figure 8(a) is shown in figure 8(b), in which the contrast from the Pt atom dominates. A large region of higher contrast from the carbon layer is visible in 8(b), showing that at 60kV it is possible to differentiate the clean and carbon containing regions, even down to a monolayer of carbon. A 3D perspective view, figure 8(c), of the atomic structure in figure 8(a), shows the surface carbon layer on top of the MoS_2. This amorphous carbon atomic model was constructed based on the information gained from the AC-TEM image in figure 8(d), where prolonged electron beam irradiation was used to sputter away MoS_2 to open holes and reveal the underlying carbon monolayer. The orange arrow in figure 8(d) indicates the monolayer amorphous carbon that contains a combination of hexagons and non-hexagonal rings. Thicker bilayer region is found just below this arrow. Pt atoms are likely to be bonded either in-plane to the carbon structure, or sit on top of the defective area. The simulations in figure 8(b) are for Pt atoms bonded in plane, as can be seen in more detail in figure 9(a)-(c).

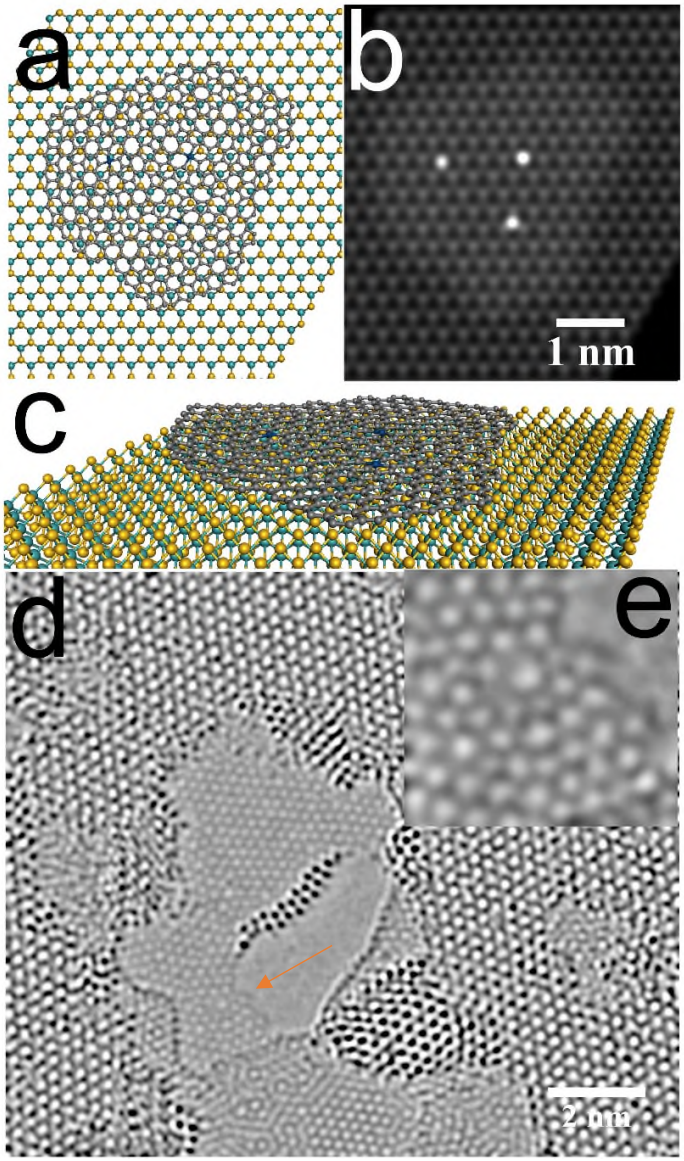

Figure 8. (a) Atomic model of MoS_2 monolayer with amorphous carbon layer on top with three Pt dopants (blue) within the carbon layer. (b) ADF-STEM images simulation based on the atomic model in (a), showing three bright contrast spots associated with the single Pt atoms in carbon. (c) 3D perspective view of the atomic model from (a). (d) AC-TEM image of monolayer MoS_2 after extensive electron beam irradiation to open up holes in the MoS_2 and reveal the surface carbon layer. Orange arrow indicates the carbon region shown in higher magnification in (e).

The amorphous nature of the carbon layer means that Pt atoms within this layer be located at random distances with respect to other Pt atoms. This will lead to the relative position of Pt atoms with respect to the Mo and S atomic columns below to be also random. The atomic models and image simulations in figures 9(d)-(i) show the variable position of Pt atoms and the resulting contrast in the image. This corresponds to images of contaminated areas of MoS_2 with Pt atoms.

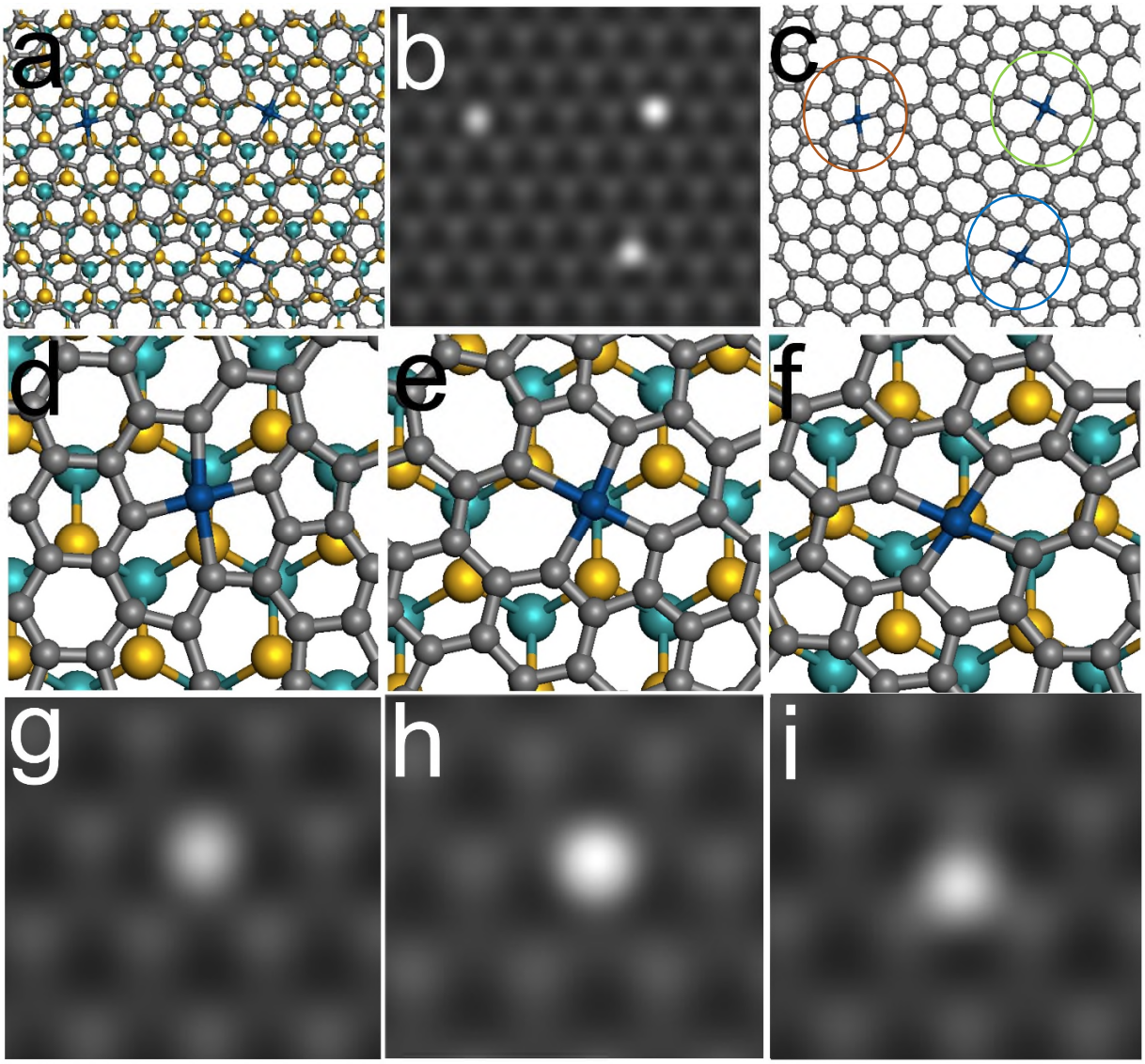

Figure 9. (a) Magnified view of the atomic model from figure 7(a), showing three Pt atoms bound within the carbon monolayer. (b) Magnified view of the ADF-STEM image simulation from figure 7(b),

corresponding to the atomic model in (a). (c) Atomic model from (a), but with the MoS_2 removed to show the position of Pt atoms in the carbon film. Circles indicate the location of Pt atoms (d)-(f) magnified view of the atomic model in (a) for Pt atom (blue) sites indicated by the coloured circles in (c) for (d) orange, (e) green and (f) blue respectively. (g)-(i) ADF-STEM image simulations corresponding to the atomic structures in (d)-(f) respectively.

In order to understand the configuration dependence of catalytic activity induced by Pt atoms on MoS_2 monolayers, we have estimated the hydrogen adsorption free energy (ΔG_H) using DFT simulations, which is highly correlated to the efficiency and has been successfully used as a descriptor for HER.[28,29] Consistent with previous studies,[14,30] our calculated ΔG_H for Mo substituted by Pt site and the S vacancy without Pt atoms are -0.00 and -0.06 eV respectively, much lower than that for the basal plane (2.06 eV). A similar degree of improvement can be obtained by Pt doping in the Mo-top configuration (0.03 eV), while S-top and V-top configurations are slightly less favorable with ΔG_H = 0.20 and 0.05 eV, respectively. In contrast to Mo substituted by Pt, the surrounding S atoms remain inert, and the H atom tends to be adsorbed on the Pt atom in the Mo-top configuration (Figure 10(c)). If the Pt atom is trapped by a S vacancy, however, ΔG_H substantially increases to 0.83 eV (Figure 10(a)) and thus the catalytic center is deactivated. Such significant differences between structures with the same dopant atoms originate from the sensitivity of the H atom binding strength to the surrounding chemical environment, which determines both the energy level of hybridized states and their occupations. For a Pt atom trapped in a S vacancy, the hybridization shifts Pt occupied orbitals towards the gap (Figure 10(b)), resulting in the relatively small binding energy. The opposite process occurs in the Mo-top configuration, wherein hybridization eliminates the relevant unoccupied orbitals while populating new mid-gap states (Figure 10(b)), leading to stabilization of the entire system. Interestingly, our

results suggest that while an individual S vacancy or Pt dopant may serve as an active catalytic center, the presence of both will suppress activity and thus should be avoided when optimizing materials for HER.

The HER activity for a series of representative single-metal atoms was explored by virtual screening of E_b and ΔG_H to provide general insights. In all situations, the S-sub configurations are energetically much more favorable than the others (Figure 10(e)), indicating that the metal atoms are prone to trapping by S vacancies. In contrast, both the absolute value of ΔG_H and the variation with different configurations strongly rely on the atom type, which reflects the complexity arising from the hybridization between H and metal orbitals as well as the polarization induced by adjacent S atoms. Such dependence is also distinct from that reported for the Mo substitution structure dictated by unsaturated S atoms.[14] In addition to confirming the superior performance of Pt atoms, the computational screening enables us to identify several candidates that may warrant future exploration. For example, Au, V and Zn dopants may provide desirable catalytic activity even in S-sub configurations. For defect-free MoS_2 sheets, Ag/Mn/Cr/Ti/V in Mo-top, Cr in S-top, and Cr/Cu/Mn/V in V-top configurations may also serve as catalytic centers. While simplified models for exploring the HER activity should be interpreted only qualitatively, the predicted diversity in performance opens an opportunity to create new catalytic centers through the rational control of dopant configuration.

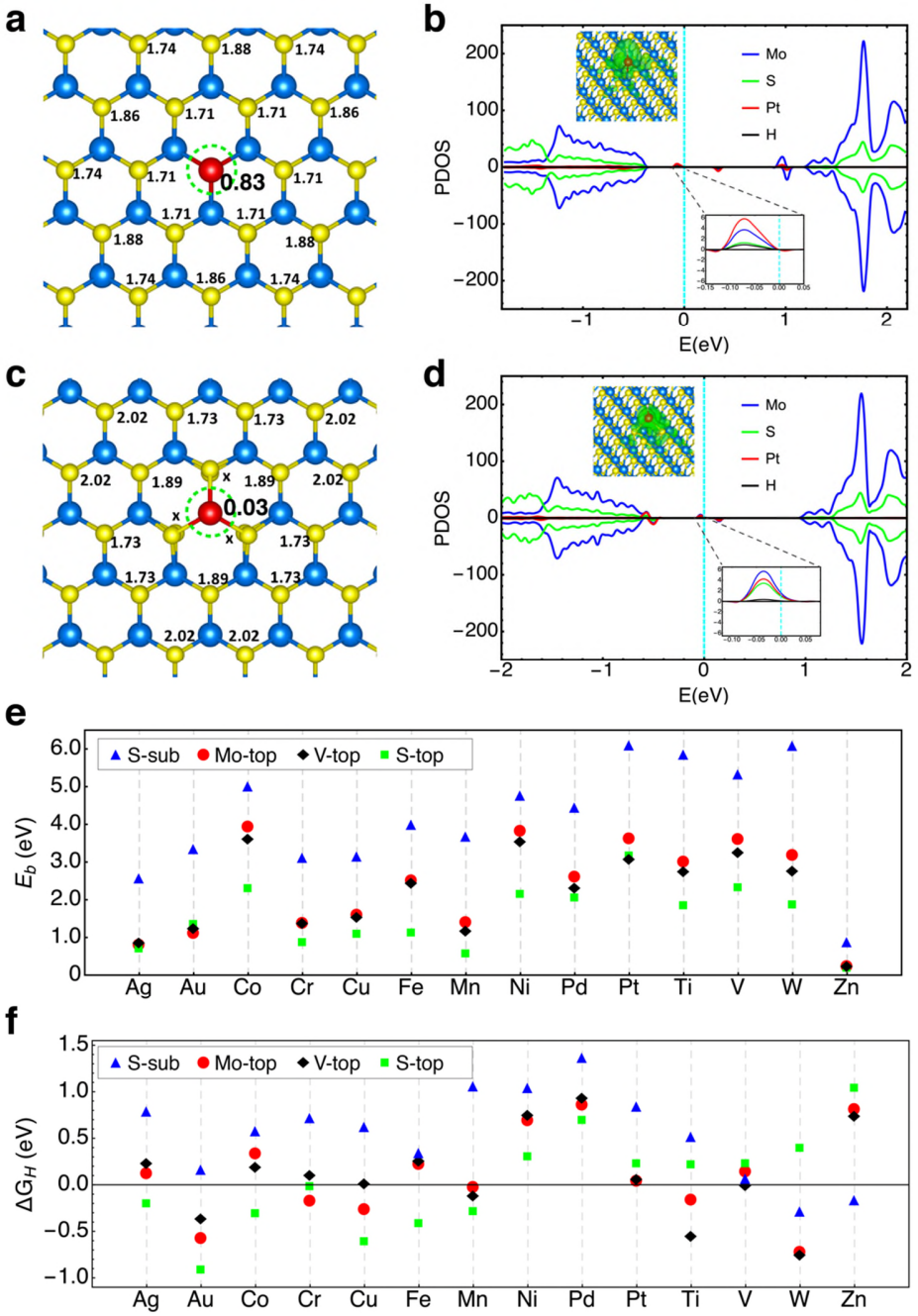

Figure 10. Calculated catalytic properties for Pt doped MoS_2 in various configurations. Hydrogen adsorption free energy (ΔG_H) in unit of eV for (a) S-sub and (c) Mo-top configurations. The green dashed circle highlights the active site for HER, while "x" means unable to bind H. Panel (b) and (d) show the spin-dependent projected density of states (PDOS) for S-sub and Mo-top configurations respectively, with

the Fermi level illustrated by the cyan dashed line. The wavefunction and detailed PDOS of the states relevant to the binding strength of H atom are shown in the inset. (e) Binding energy (E_b) and (f) ΔG_H for a series of metal atom dopant in S-sub, M-top, V-top and S-top configurations.

In summary, we have shown that isolated Pt atoms on pristine MoS2 monolayers are stabilized by bonding within S vacancies. This increases the barrier for escape and localizes Pt atoms for sufficiently long for atomic level ADF-STEM imaging. The electron beam causes hopping of Pt atoms to different S vacancy sites created by the electron beam. A different behavior is observed when Pt atoms are surrounded by carbon, in particular where a thin amorphous layer of carbon is found on the MoS_2. This layer most likely arises from the polymer transfer process and is very difficult to completely remove, as is established for graphene. However, hydrocarbons are also likely to adsorb to the MoS_2 and hence its role should always be considered when determining the structure of elements bound to the 2D material surface. The filling of S vacancies by Pt atoms has a detrimental effect on the surface catalytic activity for HER. The high mobility of Pt across the pristine surface of MoS_2 indicates that unbound Pt atoms detaching from larger Pt nanoclusters may get trapped in these vacancy sites.

Experimental Methods

Synthesis and transfer of monolayer MoS_2

MoS_2 monolayers were synthesized by a hydrogen-free CVD method using molybdenum trioxide (MoO_3, ⩾99.5%, Sigma-Aldrich) and sulphur (S, ⩾99.5%, Sigma-Aldrich) powder as precursors, as reported previously.[31] The growth was conducted under atmospheric pressure with the carrier gas of argon and SiO_2/Si (300 nm thick SiO_2) chips were used as substrates. To avoid cross-

contamination between MoO_3 and S during the reaction, an inner tube with a smaller diameter was applied to load MoO_3, which separated it from the S powder placed in the outer 1-inch quartz tube. Two furnaces were used to give a better temperature control of both precursors and the substrate. The typical heating temperature for S, MoO_3 and SiO_2/Si substrate were set to be ~ 180, ~300, and ~800 °C, respectively. After growth, monolayer MoS_2 was transferred onto a Si_3N_4 TEM grid (Agar Scientific AG21580). It was then spin-coated with a thin film of poly (methyl methacrylate) (PMMA) on the MoS_2/SiO_2/Si substrate surface, followed by floatation on a 1 mol/L potassium hydroxide (KOH) solution to etch the SiO_2. Once the PMMA/MoS_2 film was detached from the Si substrate, it was transferred to deionized water several times to remove residuals left by the etchant. Subsequently, the PMMA/MoS_2 film was transferred onto a holey Si_3N_4 TEM grid, air-dried for overnight and baked at 180 ^{0}C for 15 minutes. The PMMA scaffold was finally removed by submerging the TEM grid in acetone for 8 hours.

Sample preparation of Pt-doped monolayer MoS_2

After transferring MoS_2 single layers to a Si_3N_4 TEM grid, one drop of 0.025mol/L hexachloroplatinic acid (H_2PtCl_6)-ethanol solution was deposited onto the MoS_2 surface and dried in air. The sample was subsequently placed in a 1-inch quartz tube and heated to 350°C for 15 min with argon used as the carrier gas, which decomposed H_2PtCl_6 to Pt. After the reaction, the sample was rapidly cooled down by being removed from the hot zone furnace.

Scanning transmission electron microscopy and image processing

Room temperature ADF-STEM imaging was conducted using an aberration corrected JEOL ARM300CF STEM equipped with a JEOL ETA corrector[32] operated at an accelerating voltage of 60 kV located in the electron Physical Sciences Imaging Centre (ePSIC) at Diamond Light Source.

Dwell times of 5−20 μs and a pixel size of 0.006 nm px^{-1} were used for imaging. Optical conditions used a CL aperture of 30 μm, a convergence semi-angle of 31.5 mrad, a beam current of 44 pA, and inner-outer acquisition angles of 49.5−198 mrad.

Images were processed using the ImageJ software. A fire false colour LUT was applied to grayscale images for visual enhancement. Atomic models were generated by using Accelrys Discovery Studio Visualizer. Multislice HAADF image simulations based on the corresponding atomic models were carried out using the JEMS software with parameter settings adjusted to match the experimental conditions.

Computational Methods

Reaction path calculation

Standard ab-initio simulations within the framework of density-functional theory (DFT), as implemented in the Vienna Ab Initio Simulation Package (VASP v5.4),[33] were performed to explore the reaction paths for diffusion of Pt and S atoms on the MoS_2 monolayer. Plane-wave and projector-augmented-wave (PAW) type pseudopotentials were employed,[34] with kinetic-energy cutoffs set to 300 eV. The GGA-PBE functional[35] was used to describe the exchange-correlation interactions, while the Van der Waals effects were accounted by DFT-D2 method of Grimme,[36] with a 50 Å cutoff radius for pair interactions. The 8×4 rectangular supercells containing 192 atoms along with a 15 Å vacuum perpendicular to the sheet were constructed to prevent artificial interactions between periodic images. The minimum energy paths were determined by the climbing image nudged elastic band (CI-NEB)[37] method with 5-7 images. Only the Γ point was sampled, and the force tolerance for convergence was set to 0.03 eV/ Å.

Catalytic activity for HER

The catalytic activities of a range of metal atom dopants in different configurations were investigated by evaluating the adsorption free energy (ΔG_H), adopting an approach described in previous studies[38]

$$\Delta G_H = E(MoS_2 + H) - E(MoS_2) - E(H_2)/2 + 0.24$$

where $E(MoS_2 + H)$ and $E(MoS_2)$ are the energies of pristine or doped MoS_2 with and without an adsorbed H atom, $E(H_2)$ is the energy of a hydrogen molecule, and the term 0.24 eV accounts for the changes in zero-point energy and entropy at standard conditions. The structures were relaxed until all forces were smaller than 0.05 eV/ Å. Only the Γ point was used for geometric optimization, while a Monkhorst-Pack[39] k-point grid of 4×4×1 was applied to calculate the density of states.

The dependence of our predictions on exchange-correlation functional has been examined by Pt doped MoS_2 using a smaller 6×3 supercell. The binding energies of a Pt atom at sites of S-sub, Mo-top, S-top, V-top are predicted to be 6.22, 3.48, 3.10, 2.89 eV with HSE06 hybrid functional,[40] while those obtained by PBE functional are 6.09, 3.59, 3.09, 3.03 eV, respectively. The value of ΔG_H in these configurations calculated with HSE06 functional (0.99, 0.22, 0.12, 0.22 eV) are also consistent with those obtained with PBE functional (0.83, 0.04, 0.20, 0.05 eV), verifying that our approach is sufficient for qualitatively predicting the structural and catalytic properties.

Reference

(1) Deng, D.; Novoselov, K. S.; Fu, Q.; Zheng, N.; Tian, Z.; Bao, X. Catalysis with Two-Dimensional Materials and Their Heterostructures. *Nat. Nanotechnol.* **2016**, *11*, 218–230.

(2) Wang, H.; Wang, Q.; Cheng, Y.; Li, K.; Yao, Y.; Zhang, Q.; Dong, C.; Wang, P.; Schwingenschlögl, U.; Yang, W.; Zhang, X. X. Doping Monolayer Graphene with Single Atom Substitutions. *Nano Lett.* **2012**, *12*, 141–144.

(3) Zhang, K.; Feng, S.; Wang, J.; Azcatl, A.; Lu, N.; Addou, R.; Wang, N.; Zhou, C.; Lerach, J.; Bojan, V.; Kim, M. J.; Chen, L.-Q.; Wallace, R. M.; Terrones, M.; Zhu, J.; Robinson, J. A. Manganese Doping of Monolayer MoS_2: The Substrate Is Critical. *Nano Lett.* **2015**, *15*, 6586–6591.

(4) Yun, W. S.; Lee, J. D. Unexpected Strong Magnetism of Cu Doped Single-Layer MoS_2 and Its Origin. *Phys. Chem. Chem. Phys.* **2014**, *16*, 8990–8996.

(5) Robertson, A. W.; Montanari, B.; He, K.; Kim, J.; Allen, C. S.; Wu, Y. a.; Olivier, J.; Neethling, J.; Harrison, N.; Kirkland, A. I.; Warner, J. H. Dynamics of Single Fe Atoms in Graphene Vacancies. *Nano Lett.* **2013**, *13*, 1468–1475.

(6) Ma, D.; Ju, W.; Li, T.; Zhang, X.; He, C.; Ma, B.; Lu, Z.; Yang, Z. The Adsorption of CO and NO on the MoS_2 Monolayer Doped with Au, Pt, Pd, or Ni: A First-Principles Study. *Appl. Surf. Sci.* **2016**, *383*, 98–105.

(7) Chen, Q.; Robertson, A. W.; He, K.; Gong, C.; Yoon, E.; Kirkland, A. I.; Lee, G.-D.; Warner, J. H. Elongated Silicon–Carbon Bonds at Graphene Edges. *ACS Nano* **2016**, *10*, 142–149.

(8) Cao, C.; Wu, M.; Jiang, J.; Cheng, H. P. Transition Metal Adatom and Dimer Adsorbed on Graphene: Induced Magnetization and Electronic Structures. *Phys. Rev. B* **2010**, *81*, 205424.

(9) Chan, K. T.; Neaton, J. B.; Cohen, M. L. First-Principles Study of Metal Adatom Adsorption on Graphene. *Phys. Rev. B* **2008**, *77*, 235430.

(10) Cong, W. T.; Tang, Z.; Zhao, X. G.; Chu, J. H. Enhanced Magnetic Anisotropies of Single Transition-Metal Adatoms on a Defective MoS_2 Monolayer. *Sci. Rep.* **2015**, *5*, 9361.

(11) Zhang, X.; Lu, Z.; Xu, G.; Wang, T.; Ma, D.; Yang, Z.; Yang, L. Single Pt Atom Stabilized on Nitrogen Doped Graphene: CO Oxidation Readily via the Tri-Molecular Eley-Rideal Mechanism. *Phys. Chem. Chem. Phys.* **2015**, *17*, 20006–20013.

(12) Qiao, B.; Wang, A.; Yang, X.; Allard, L. F.; Jiang, Z.; Cui, Y.; Liu, J.; Li, J.; Zhang, T. Single-Atom Catalysis of CO Oxidation Using Pt_1/FeO_x. *Nat. Chem.* **2011**, *3*, 634–641.

(13) Cheng, N.; Stambula, S.; Wang, D.; Banis, M. N.; Riese, A.; Xiao, B.; Li, R.; Sham, T.-K.; Liu, L.; Botton, G. A.; Sun, X. Platinum Single Atom and Cluster Catalysis of the Hydrogen Evolution Reaction. *Nat. Commun.* **2016**, *7*, 13638.

(14) Deng, J.; Li, H.; Xiao, J.; Tu, Y.; Deng, D.; Yang, H.; Tian, H.; Li, J.; Ren, P.; Bao, X. Triggering the Electrocatalytic Hydrogen Evolution Activity of Inert Two-Dimensional MoS_2 Surface via Single-Atom Metal Doping. *Energy Environ. Sci.* **2015**, *8*, 1594–1601.

(15) Dai, X.; Du, K.; Li, Z.; Liu, M.; Ma, Y.; Sun, H.; Zhang, X.; Yang, Y. Co-Doped MoS_2 Nanosheets with the Dominant CoMoS Phase Coated on Carbon as an Excellent Electrocatalyst for Hydrogen Evolution. *ACS Appl. Mater. Interfaces* **2015**, *7*, 27242–27253.

(16) Krivanek, O. L.; Chisholm, M. F.; Nicolosi, V.; Pennycook, T. J.; Corbin, G. J.; Dellby, N.; Murfitt, M. F.; Own, C. S.; Szilagyi, Z. S.; Oxley, M. P.; Pantelides, S. T.; Pennycook, S. J. Atom-by-Atom Structural and Chemical Analysis by Annular Dark-Field Electron Microscopy. *Nature* **2010**, *464*, 571–574.

(17) Warner, J. H.; Lin, Y.; He, K.; Koshino, M.; Suenaga, K. Stability and Spectroscopy of Single Nitrogen Dopants in Graphene at Elevated Temperatures. *ACS Nano* **2014**, *8*, 11806–11815.

(18) Lin, Y. C.; Teng, P. Y.; Yeh, C. H.; Koshino, M.; Chiu, P. W.; Suenaga, K. Structural and Chemical Dynamics of Pyridinic-Nitrogen Defects in Graphene. *Nano Lett.* **2015**, *15*, 7408–7413.

(19) Lin, Y. C.; Dumcenco, D. O.; Komsa, H.-P.; Niimi, Y.; Krasheninnikov, A. V.; Huang, Y.-S.; Suenaga, K. Properties of Individual Dopant Atoms in Single-Layer MoS_2: Atomic Structure, Migration, and Enhanced Reactivity. *Adv. Mater.* **2014**, *26*, 2857–2861.

(20) Robertson, A. W.; Lin, Y.; Wang, S.; Sawada, H.; Allen, C. S.; Chen, Q.; Lee, S.; Lee, G.; Han, S.; Yoon, E.; Kirkland, A. I.; Kim, H.; Suenage, K.; Warner, J. H. Atomic Structure and Spectroscopy of Single Metal (Cr, V) Substitutional Dopants in Monolayer MoS_2. *ACS Nano* ***2016****, 10, 10227–10236.*

(21) Chen, Q.; He, K.; Robertson, A. W.; Kirkland, A. I.; Warner, J. H. Atomic Structure and Dynamics of Epitaxial 2D Crystalline Gold on Graphene at Elevated Temperatures. *ACS Nano* **2016**, *10*, 10418–10427.

(22) Wang, S.; Lee, G.-D.; Lee, S.; Yoon, E.; Warner, J. H. Detailed Atomic Reconstruction of Extended Line Defects in Monolayer MoS_2. *ACS Nano* **2016**, *10*, 5419–5430.

(23) Komsa, H.-P.; Kurasch, S.; Lehtinen, O.; Kaiser, U.; Krasheninnikov, A. V. From Point to Extended Defects in Two-Dimensional MoS_2: Evolution of Atomic Structure under Electron Irradiation. *Phys. Rev. B* **2013**, *88*, 35301.

(24) Zan, R.; Ramasse, Q. M.; Jalil, R.; Georgiou, T.; Bangert, U.; Novoselov, K. S. Control of Radiation Damage in MoS_2 by Graphene Encapsulation. *ACS Nano* **2013**, *7*, 10167–10174.

(25) Komsa, H.-P.; Kotakoski, J.; Kurasch, S.; Lehtinen, O.; Kaiser, U.; Krasheninnikov, A. V. Two-Dimensional Transition Metal Dichalcogenides under Electron Irradiation: Defect Production and Doping. *Phys. Rev. Lett.* **2012**, *109*, 35503.

(26) Komsa, H.P.; Kotakoski, J.; Kurasch, S.; Lehtinen, O.; Kaiser, U; Krasheninnikov, A.V. Two-dimensional Transition Metal Dichalcogenides under Electron Irradiation: Defect Production and Doping. *Phys. Rev. Lett.* **2012,** *109*, 035503.

(27) Garcia, A.; Raya, A.M.; Mariscal, M.M.; Esparza, R.; Herrera; M., Molina; S.I., Scavello; G., Galindo; P.L., Jose-Yacaman; M. and Ponce, A. Analysis of Electron Beam Damage of Exfoliated MoS2 Sheets and Quantitative HAADF-STEM Imaging. *Ultramicroscopy* **2014,** *146*, 33-38.

(28) Greeley, J.; Mavrikakis, M. Alloy Catalysts Designed from First Principles. *Nat. Mater.* **2004**, *3*, 810–815.

(29) Tsai, C.; Abild-Pedersen, F.; Nørskov, J. K. Tuning the MoS_2 Edge-Site Activity for Hydrogen Evolution via Support Interactions. *Nano Lett.* **2014**, *14*, 1381–1387.

(30) Li, H.; Tsai, C.; Koh, A. L.; Cai, L.; Contryman, A. W.; Fragapane, A. H.; Zhao, J.; Han,

H. S.; Manoharan, H. C.; Abild-Pedersen, F.; Norskov, J. K.; Zheng, X. L. Activating and Optimizing MoS2 Basal Planes for Hydrogen Evolution through the Formation of Strained Sulphur Vacancies. *Nat. Mater.* **2015**, *15*, 48–53.

(31) Wang, S.; Wang, X.; Warner, J. H. All Chemical Vapor Deposition Growth of MoS_2:h-BN Vertical van Der Waals Heterostructures. *ACS Nano* **2015**, *9*, 5246–5254.

(32) Hosokawa, F.; Sawada, H.; Kondo, Y.; Takayanagi, K.; Suenaga, K. Development of Cs and Cc Correctors for Transmission Electron Microscopy. *Microscopy* **2013**, *62*, 23–41.

(33) Kresse, G.; Furthmüller, J. Efficient Iterative Schemes for Ab Initio Total-Energy Calculations Using a Plane-Wave Basis Set. *Phys. Rev. B* **1996**, *54*, 11169–11186.

(34) Blochl, P. E. Projector Augmented-Wave Method. *Phys. Rev. B - Condens. Matter Mater. Phys.* **1994**, *50*, 17953–17979.

(35) Perdew, J. P.; Burke, K.; Ernzerhof, M. Generalized Gradient Approximation Made Simple. *Phys. Rev. Lett.* **1996**, *77*, 3865–3868.

(36) Grimme, S. Semiempirical GGA-Type Density Functional Constructed with a Long-Range Dispersion Correction. *J. Comput. Chem.* **2006**, *27*, 1787−1799.

(37) Henkelman, G.; Uberuaga, B. P.; Jónsson, H. A Climbing Image Nudged Elastic Band Method for Finding Saddle Points and Minimum Energy Paths. *J. Chem. Phys.* **2000**, *113*, 9901–9904.

(38) Nørskov, J. K.; Bligaard, T.; Logadottir, A.; Kitchin, J. R.; Chen, J. G.; Pandelov, S.; Stimming, U. Trends in the Exchange Current for Hydrogen Evolution. *J. Electrochem. Soc.* **2005**, *152*, J23–J26.

(39) Monkhorst, H. J.; Pack, J. D. Special Points for Brillouin-Zone Integrations. *Phys. Rev. B* **1976**, *13*, 5188–5192.

(40) Krukau, A.V.; Vydrov; O.A., Izmaylov; A.F. and Scuseria; G.E. Influence of the Exchange Screening Parameter on the Performance of Screened Hybrid Functionals. *J. Chem. Phys.* **2006,** 125, 224106.

TOC Graphic